Kinetik: Game Technology, Information System, Computer Network, Computing, Electronics, and Control
Journal homepage: http://kinetik.umm.ac.id
ISSN: 2503-2267
Vol. 10, No. 2, May, Pp. 135-148

Improvement of AC bus voltage stability with current control inverter

Bayu Rahmad Nugroho*[1], Reza Maulidin[1], Adhi Kusmantoro[1]
Department of Electrical Engineering, Universitas PGRI Semarang, Indonesia[1]

Article Info
Keywords:
Current control, Inverter, PV Array, Fuzzy Logic

Article history:
Received: August 29, 2024
Accepted: December 27, 2024
Published: May 31, 2025

Cite:
B. R. Nugroho, R. Maulidin, and A. Kusmantoro, "Improvement of AC Bus Voltage Stability with Current Control Inverter ", *KINETIK*, vol. 10, no. 2, May 2025. https://doi.org/10.22219/kinetik.v10i2.2107

*Corresponding author.
Bayu Rahmad Nugroho
E-mail address:
rahmadbayu749@gmail.com

Abstract
This research focuses on the development and analysis of a current control method for inverters, which demonstrates superior performance compared to the more conventional voltage control method. Current control in inverters offers several significant advantages, including faster dynamic response, constant switching frequency, and the ability to effectively reduce harmonic distortion, which is often a challenge in modern power systems. Additionally, this method is capable of maintaining system stability even when it had complex load variations and fluctuating operating conditions. In this study, we implement a fuzzy logic approach to simulate current control in an inverter integrated with a photovoltaic (PV) renewable energy system. The simulation results indicate that the proposed current control method not only enhances overall energy efficiency, but also extends the operating range of the inverter, allowing the system to operate optimally under various load conditions.

1. Introduction

With technological advancements and the growing need for stable electricity, inverter control techniques in microgrids have become crucial, especially due to the depletion of fossil fuels. Microgrids, utilizing renewable energy, help meet the community's stable electricity needs. This research focuses on distributed power generation and converter development. A control inverter is an inverter equipped with a control mechanism to regulate the output voltage, current, or frequency according to the specific needs of an application. This control can be implemented through various techniques, such as vector control, current control, or voltage control, to ensure that the inverter produces a stable output that meets the desired parameters. Control inverters are widely used in motor drives, power systems, and distributed power applications to achieve optimal efficiency and performance. The implementation of parabolic current control in voltage source inverters is discussed in this section. Several advantages of parabolic current control are explained, including fast response and constant switching frequency, as well as improved system performance by reducing waveform distortion[1].

The method to reduce internal resonance circulation current (IRCC) and external resonance circulation current (ERCC) in three-level parallel inverters with a modified LCL filter is discussed. The explanation includes the causes of current instability and the zero-sequence circulating current (ZSCC) control method to address this issue[2],[3]. Two new model predictive current control (MPCC) methods for single-phase voltage source inverters (VSI) are also presented. In one sampling period, this technique controls the output current using two different output voltages with varying application durations[4]. A cost-effective four-wire current source inverter with separate capacitors is introduced. It significantly reduces common mode voltage (CMV) and addresses leakage current issues by connecting the DC link midpoint to the neutral point of the AC filter capacitor[5]. A current control approach for Vehicle-to-Grid (V2G) technology using a three-phase four-leg inverter with an LCL filter is also discussed. This approach combines a deadbeat controller (DB), based on a weighted average inductor current (WAIC) scheme, with a repetitive controller (RC) to address system delays and uncertainties[6]. Compensation for parabolic current control in voltage source inverters that addresses dead time effects is also covered. This method improves current tracking and extends the duty cycle range, with its effectiveness verified through experiments on a full-bridge inverter[7]. A hysteresis current control method for grid-tied inverters that eliminates AC current sensors by using DC link voltage and grid voltage to calculate switching instants is also explored[8],[9]

A new current sensor that combines a current transformer and a commercial sensor is proposed for accurately measuring and suppressing DC current injection in transformerless grid-connected inverters. The proposed sensor reduces cost, volume, and measurement errors, with its effectiveness validated through experiments on a 1.5 kVA inverter[10]. Two effective MPCC schemes for five-phase voltage source inverters are suggested in this article. The MPCC-V3-RCMV1 reduces harmonics, while the MPCC-V3-RCMV2 reduces switching frequency[11]. A new control

method called triple-voltage-vector model-free predictive current control (TVV-MFPCC) is introduced for four-switch three-phase (FSTP) inverters that drive surface-mounted permanent magnet synchronous motors (SPMSM). This technique enhances voltage vector selection using discrete space vector modulation (DSVM) while reducing redundant calculations through a specific scheme[12]. The application of variable-frequency pulse width modulation (VFPWM) in an average current mode control with variable frequency for a dual-buck H-bridge (DBHB) inverter with quasi-square wave (QSW) zero-voltage switching (ZVS) using GaN devices is discussed[13]. A closed-loop time-domain model is developed to analyze fault current characteristics in three-phase three-leg inverters under unsymmetrical faults[14]. A simple method is developed to reduce grid current harmonics in voltage source inverters using an LCL filter with inverter-side current feedback (ICF) control [15]. A new model predictive current control (MPCC) scheme is designed to reduce common-mode voltage (CMV) and current harmonics in two-level seven-phase voltage source inverters (VSI)[16]. An improved continuous control set model predictive control (CCS-MPC) scheme enhanced by a fuzzy logic approach (FLA) is proposed for three-phase inverters with constant voltage constant frequency (CVCF) using an LC output filter[17]. A new approach is introduced to enhance finite control set model predictive current control (FCS-MPCC) in three-phase and five-phase voltage source inverters (VSI). The effectiveness of this method is validated through simulation and experimental results, demonstrating its advantages over existing FCS-MPCC methods in terms of structural simplicity, dynamic performance, constant switching frequency, and minimal current ripple[18]. A new sensorless voltage detection method is introduced for direct current control in grid-connected multilevel inverters using a scalar hysteresis controller (SHC). This method emphasizes the simplicity and flexibility of SHC in handling various levels of multilevel inverters, highlighting improvements in switching behavior and the reduction of current errors achieved by the proposed method[19]. The use of photovoltaic cells can convert sunlight into electricity and charge a smartphone's battery. The photovoltaic cells are integrated with the smartphone's battery in a photovoltaic IC to form a battery charging system capable of charging the smartphone. The design of the micro photovoltaic cell sensor section is based on reference papers. The micro photovoltaic cell is designed by modifying the resistor value in the micro photovoltaic cell circuit, so the low output voltage and power can be used to charge the smartphone's battery[20].

Based on the previous studies, inverter voltage control demonstrated suboptimal stability and reliability, with limitations in addressing unbalanced and nonlinear loads. Therefore, this study proposes FLC-based control, which has proven superior in various aspects. The FLC approach provides faster and more accurate responses to load variations and system disturbances. Additionally, this method is easier to implement and adapt to various operational conditions. Based on this introduction, the article's structure is organized as follows: Section 2 discusses the Research Methodology, Section 3 presents the Results and Discussion, and Section 4 concludes the study.

2. Research Method

2.1 PVA - 1

The configuration of the 3-phase grid-connected voltage-source inverter (VSI) system based on PV considered in this work is illustrated in Figure 1. The system consists of an FLC controller, PV simulator, inverter, and load. The control system includes several sub-system modules, such as voltage and current control functions, grid synchronization, pulse width modulation (PWM) signal generator, as well as detection of abnormal voltages like overvoltage and undervoltage, and frequency. By sampling output parameters such as voltage and current and applying control and MPPT algorithms, the system controller successfully transfers maximum power from the PV to the load and stabilizes the AC output voltage, current, and frequency to the desired levels. This is achieved by generating PWM signals for the inverter's switching devices. A controllable breaker is used to connect and disconnect the inverter from the grid.

The PV simulator, equipped with a dc-dc boost converter and a perturb and observe (P&O) based maximum power point tracking (MPPT) algorithm, provides the appropriate and regulated dc power for the inverter. In the P&O method, parameters such as PV voltage or current are continuously adjusted to obtain the maximum power from the PV panel. The MPPT feature allows the PV system to deliver maximum power at various levels of solar irradiation. The PV output parameters vary depending on solar irradiation and temperature. In this study, for simplicity, the implementation is carried out at a fixed solar irradiation of 1000 Watt/m² and a temperature of 25ºC. The PV module parameters include open-circuit voltage, Voc (21.8 V), short-circuit current, Isc (5 A), voltage at maximum power, Vmp (17 V), and current at maximum power, Imp (4.7 A). The PV array consists of modules connected in series and parallel to produce a total dc output voltage of 408 V with a power capacity of 5.8 kW, which is then fed to the dc-dc boost converter in Equation 1. In principle, the output voltage of the solar cell depends on the photon current affected by the level of solar irradiation during operation. The output current of the solar cell can be expressed as[21]:

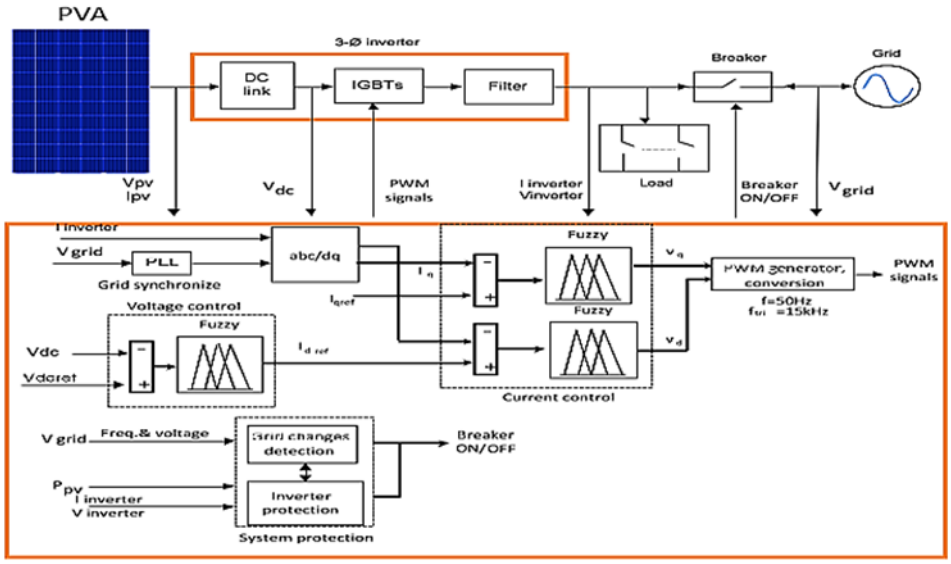

Figure 1. Fuzzy Control System

$$I_c = I_{ph} - I_0 = I_{ph} - I_{sat}\, e_{AKT}^{q}(V + IRS) - 1) \quad (1)$$

2.2 Inverter

An inverter functions to convert DC voltage into AC voltage. Inverters used in microgrids are responsible for providing AC power to loads. There are two types of inverters: grid-connected and off-grid. Grid-connected inverters require synchronization control with the grid, which is typically done using a PLL (Phase Locked Loop) circuit. To reduce harmonics in the inverter's output, filters are used[22],[23],[24]. The full-bridge PV inverter without an isolation transformer at the output is shown in Figure 2. From Figure 2, the grid current reference $\boldsymbol{i_{ref}}$ can be expressed using Equation 2.

$$i_{ref} = i_{ref} \cos \emptyset \quad (2)$$

where $\boldsymbol{i_{ref}}$ is the grid current command amplitude, and θ is the phase angle of the grid current synchronized with the grid voltage using a Phase Locked Loop (PLL). The PV inverter output typically has a DC offset due to power module disparity, pulse asymmetry, and current detection errors. Traditionally, a transformer is used between the PV inverter and the grid to prevent DC current injection. However, without an isolation transformer, the DC offset in the inverter's output can lead to significant DC current injection, which may violate grid connection standards.

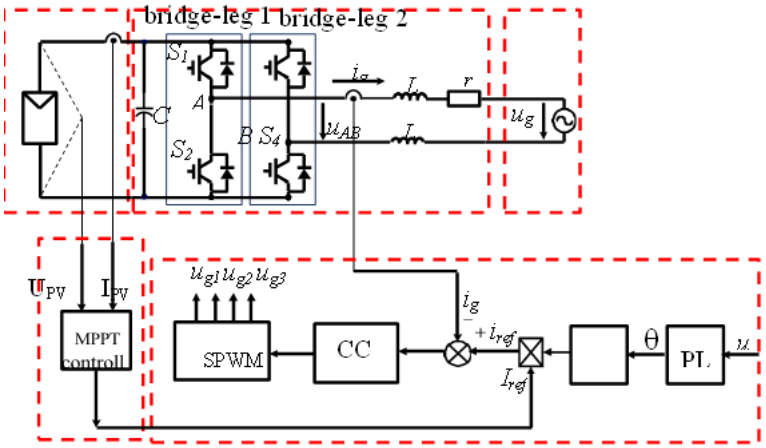

Figure 2. The Original Scheme Diagram of PV Grid-connected Inverter

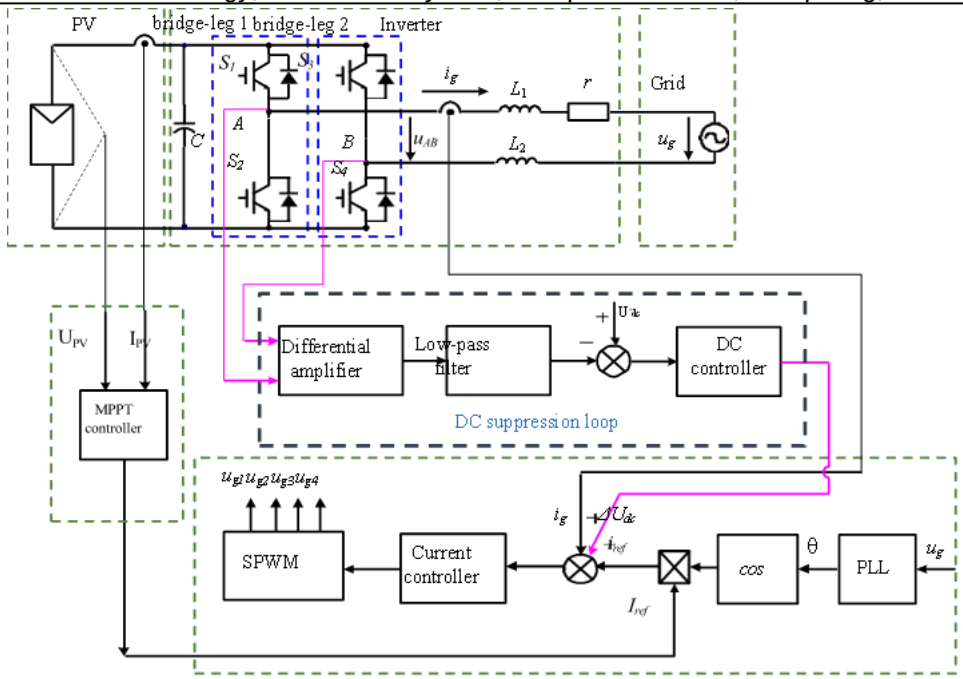

Figure 3. The Novel Scheme Diagram of PV Grid-connected Inverter

Compared to Figure 2, the new control scheme in Figure 3 is equipped with an additional loop to reduce the DC voltage. This DC suppression loop consists of a differential amplifier, a low-pass filter, and a DC controller.

The input to the DC suppression loop is u_{AB}, which is a high-frequency PWM waveform taken between point A on leg 1 and point B on leg 2 of the bridge inverter. The DC offset voltage of u_{AB} is accurately measured using a differential amplifier and a low-pass filter. Next, the DC offset voltage is compared with the DC inverter voltage reference U_{dcref}, which is set to zero, and the difference is measured. This error is then controlled by an integral controller. The output of the DC controller ΔU_{dc}, which is also the result of the DC suppression loop, is added to the grid current reference i_{ref} in the grid current control loop.

This new control strategy has two main advantages. First, a differential amplifier is used to measure the DC offset voltage between two midpoints of the full-bridge inverter[25],[26]. To accurately detect the DC offset voltage of the output voltage across the inverter switches u_{AB}, a differential amplifier with high precision, low offset, and high common-mode rejection ratio (CMRR) is required. Second, the use of this differential amplifier not only reduces costs but also prevents zero drift typically caused by Hall effects.

2.3 Method Proposed Fuzzy Logic Controller

The basic architecture of the Fuzzy Logic Controller (FLC) used in the control strategy is shown in Figure 4. The FLC system consists of several main elements: the fuzzifier unit at the input, the knowledge base (rule base) and inference engine, and the defuzzifier at the output. In an FLC-based control system, the required variables include input and output variables. The input to the FLC consists of parameters or variables from the process being controlled, depending on the application. Typically, input variables are the error and the rate of change of the error. Meanwhile, the output variables include changes in current and voltage. The error at discrete time is the difference between the desired output or reference, $r(p)$, and the process output variable, $y(p)$. The current error, $e(p)$, and the change in error, $\Delta e(p)$, are defined in Equations 3 and 4, respectively.

These variables, normalized to fall within the range of -1 to +1, require seven membership functions as shown in Figure 5. Inputs outside this range are considered too large and will result in a significant error signal. To simplify, triangular and trapezoidal membership functions are used. By using triangular and trapezoidal membership functions, the controller can reduce the error signal more quickly, thus improving the system's transient response. The membership functions are labeled as NB for ‘Negative Big’, NS for ‘Negative Small’, ZE for ‘Zero’, PS for ‘Positive Small’, and PB for ‘Positive Big’. Input variables are categorized through these membership functions.

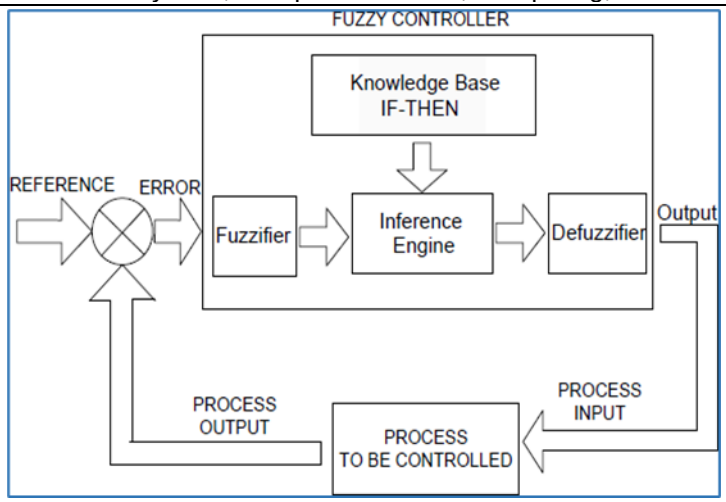

Figure 4. Fuzzy Logic Control Architecture

$$e(p) = r(p) - y(p) \tag{3}$$

$$\Delta e(p) = e(p) - e(p-1) \tag{4}$$

Based on the fundamental principles of the inference process and with the aid of knowledge-based rules, fuzzy output is generated. A key element of the Fuzzy Logic Controller (FLC) is the knowledge-based component, which contains a list of fuzzy rules. The inference process aims to produce a set of fuzzy outputs according to IF-THEN rules. By using these rules, the fuzzy controller can operate intelligently and mimic human decision-making. There are 49 'IF-THEN' logic rules related to input and output, as shown in Figure 5. This logic transforms the control functions into an FLC.

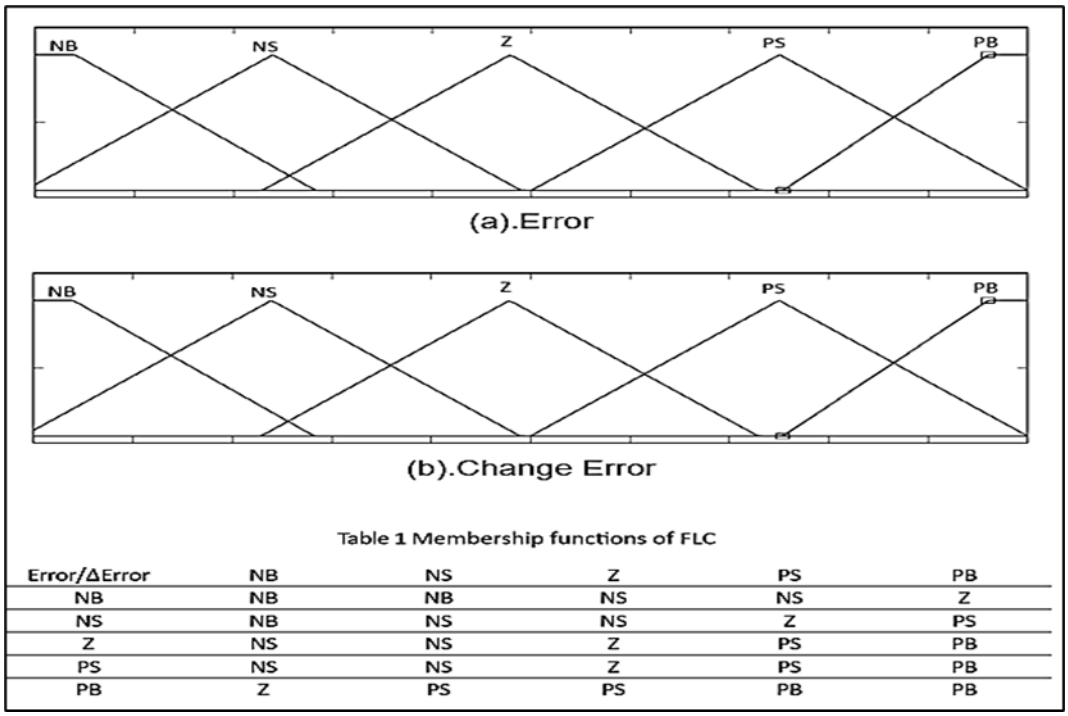

Table 1 Membership functions of FLC

Error/ΔError	NB	NS	Z	PS	PB
NB	NB	NB	NS	NS	Z
NS	NB	NS	NS	Z	PS
Z	NS	NS	Z	PS	PB
PS	NS	NS	Z	PS	PB
PB	Z	PS	PS	PB	PB

Figure 5. Membership Functions for Error, Change of Error, Controller Output and Rule Base Matrix Table

In the system implementation, the fuzzy controller output, $u(k+1)Ts$, continuously changes at each sampling time until it reaches a steady-state condition as described in Equation 5.

$$u(p+I) = u(p) + \Delta u(p) \tag{5}$$

Where $\Delta u(k)$ represents a sample of the controller output. In this study, the center of area defuzzification method is applied to determine the actual output from the fuzzy value as listed in Equation 6. This technique is simple and accurate as it finds the 'balance' point within the solution region by calculating the weighted average of the fuzzy area.

$$u = \sum i = 1\, n\, (xi \times \mu i \tag{6}$$

Where $\mu(ui)$ is the membership value of the combined membership function corresponding to each rule.

3. Results and Discussion

The prototype of the grid-connected PV inverter control system was tested under various scenarios such as load changes, voltage disturbances, and grid frequency variations. Examples of the results are presented below. During normal synchronization of the inverter with the grid, Figure 6 shows the tested waveforms of the inverter output voltage, injected current, and grid voltage for one phase over a period of 0.16 seconds with a sampling interval of 5 µs.

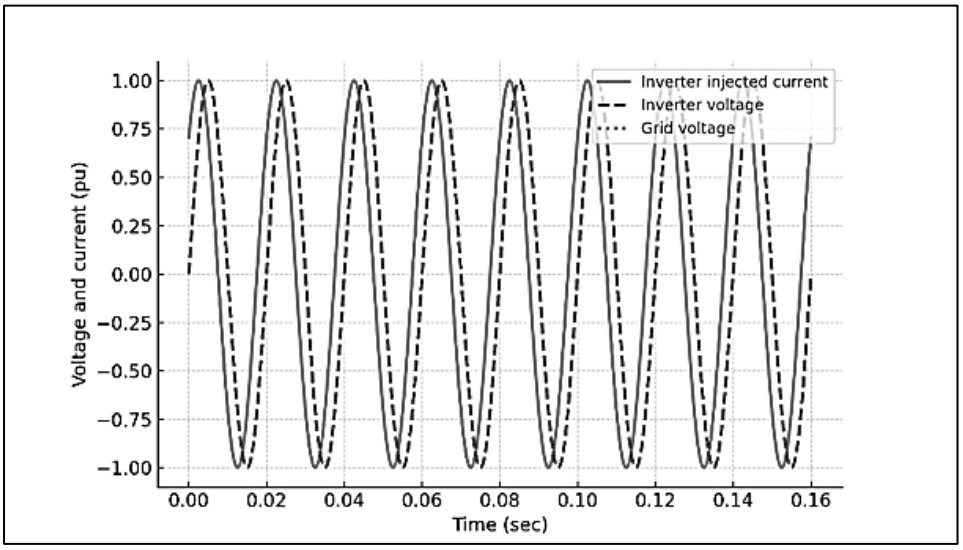

Figure 6. Inverter Injected Current, Inverter Voltage and Grid Voltage

The figure shows that the waveform displayed is nearly sinusoidal with a frequency of 50 Hz and a peak voltage of 1.0 p.u. This voltage is equivalent to a phase RMS voltage of 240 V or a line voltage of 415 V. Initially, the system operates in standalone mode as a voltage-controlled inverter. Subsequently, the inverter adjusts to the frequency and phase of the grid, allowing it to connect to the grid. After successful synchronization, the grid connection switch is closed and the system begins operating in grid-connected mode at 0.03 seconds, functioning as a current-controlled inverter. This is an essential feature for grid-connected PV inverters to ensure a secure connection. The voltage is kept stable during the connection process to ensure a constant power flow to the grid. The injected current matches the grid voltage (unity power factor) although there is a slight delay at the start of the connection due to the control algorithm. In grid-connected mode, the system uses a current control scheme, and the reference current tracking shows very little ripple in the current waveform. The Fuzzy Logic Controller (FLC) functions to maintain a stable injected current, as indicated by the stability of the current waveform. Thus, the inverter is able to transfer constant PV power to the grid and load.

Understanding the power flow in a grid-connected PV inverter system is crucial. The power flow of this inverter system is illustrated in Figure 7. During the period from 0 to 0.05 seconds, with a load demand of 5.8 kW, considered as a 100% load scenario, almost no power is fed into the grid. This occurs because of a power balance between PV and the load, where the power generated matches the power demand. When the system is in grid-connected mode, from 0.05 to 0.1 seconds, the load power increases to 8.8 kW, which is considered a 150% load scenario, equivalent to 3 kW increase. In this condition, the load requires more power from the PV system. Since the PV capacity is 5.8 kW, the additional 3 kW is drawn from the grid, as indicated by the -3 kW value on the grid contribution profile in the figure. The grid continues to supply power to the load until 0.1 seconds, when the load decreases to 3.0 kW. This is referred to as a 50% load scenario, where the load uses less power than what is generated. Therefore, the excess PV power of approximately 3 kW is fed into the grid, as shown by the +3.0 kW value on the grid contribution profile line. This power flow analysis demonstrates the inverter's ability to draw power from the PV system and distribute it to the load and the grid.

When the inverter transitions from standalone mode to grid-connected mode, a small step transient condition is observed as depicted in Figure 9. However, the designed FLC controller is able to handle the transient effects effectively, and the system quickly returns to a stable state. This brief transient is caused by challenges in tuning the FLC and the curse of dimensionality associated with rule formulation.

In general, grid-connected systems experience highly variable transient conditions. Grid-connected PV systems can manage power fluctuations from solar radiation as well as variations in frequency and system load. It is observed that with a PI controller, the inverter system exhibits significant transients and overshoot in the power generated by the PV and the power contribution from the grid compared to the FLC controller, as shown in Figure 6(a). However, the designed FLC controller can effectively handle transient effects, and the system quickly returns to a stable state, as seen in Figure 6(b). These brief transients arise due to challenges in tuning the FLC and the curse of dimensionality in rule formulation.

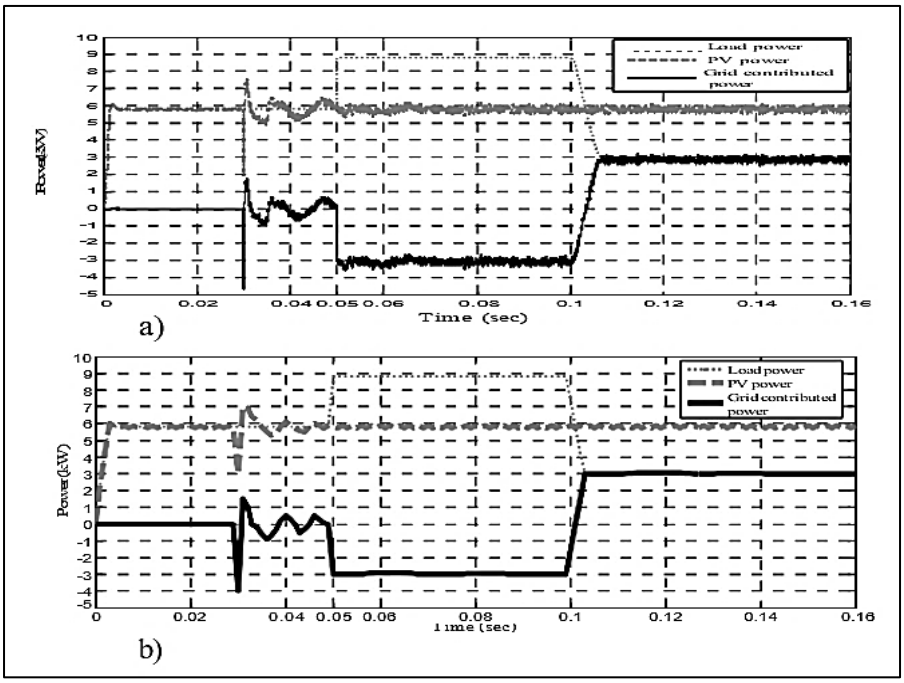

Figure 7. Inverter System Power Flow Using a) PI Controller b) FLC Controller

Figure 8 shows the voltage and current waveforms of the load during changes in load demand. Both waveforms are aligned during the load variation period. When the load power demand exceeds the PV capacity, additional power is drawn from the grid, as seen in the current waveform between 0.05 and 0.1 seconds. After 0.1 seconds, the decrease in load power demand leads to a reduction in load current. As a result, the excess PV power is fed into the grid. Importantly, the load voltage remains stable despite changes in the load power profile, ensuring a consistent power flow to both the load and the grid.

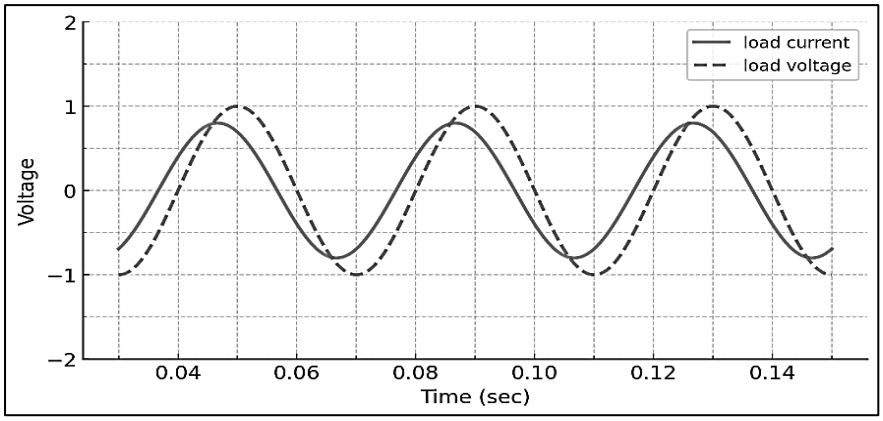

Figure 8. Load Voltage and Current Waveforms During Load Demand Variation

Ensuring high-quality output power with low harmonic content in voltage and current is important, especially when it is connected to the power grid. Using Fast Fourier Transform (FFT) techniques, the Total Harmonic Distortion (THD) of the phase voltage and current waveforms is calculated to be 2.48% and 4.64%, respectively. These values are below the 5% limit set by IEEE Std. 929-2000. The waveforms and related harmonic spectra can be seen in Figures 9 and 10. This level of harmonics is achieved due to the effectiveness of the control algorithm, which combines FLC, SPWM techniques, voltage and current control algorithms, and the use of filters.

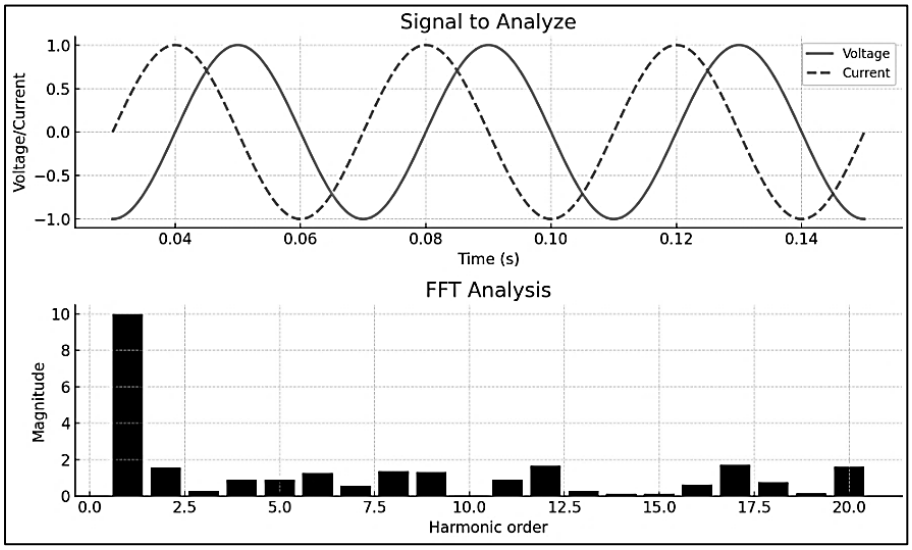

Figure 9. THD and Harmonics Spectrum of Inverter Output Voltage

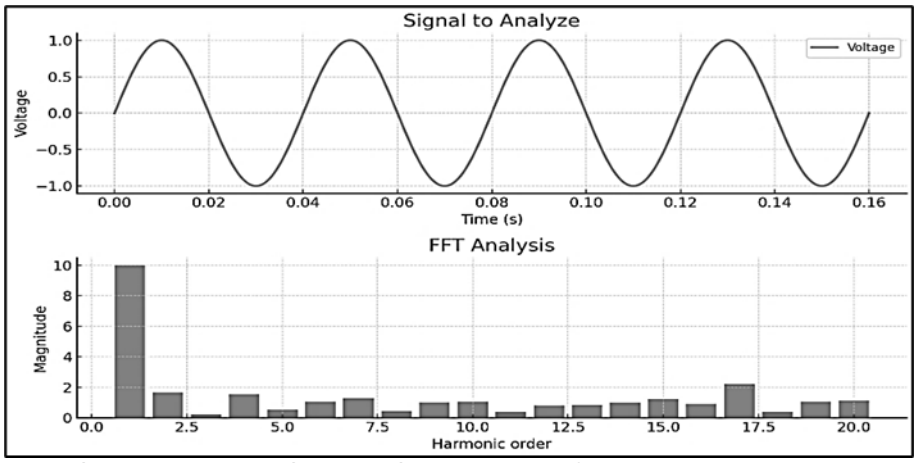

Figure 10. THD and Harmonics Spectrum of Inverter Output Current

The performance of the FLC and PI controllers is evaluated based on the transient response and stability in maintaining the DC link voltage to keep the ripple in the inverter's AC output waveform low. In standalone mode, the FLC demonstrates good response without overshoot during the early transient stage, as shown in Figure 11. In contrast, the transient response of the PI controller exhibits overshoot initially before reaching a stable condition, which can be seen in Figure 12. The steady-state response for grid-connected mode is considered satisfactory for both controllers, as observed after t = 0.04 seconds.

The behavior of the inverter during grid disturbances such as overvoltage, undervoltage, over-frequency, and under-frequency is shown in the following figures. These disturbances are intentionally applied to assess the inverter's control algorithm capabilities in handling disturbances in a safe and effective manner. The response is tested based on the criteria that the inverter should stop supplying power to the grid if the grid voltage exceeds 110% (264 V) or drops below 88% (211 V) of the nominal voltage of 240 V. For frequency, the inverter system is evaluated when the frequency exceeds 51 Hz or drops below 49 Hz. These disturbances are applied during the time period between 0.06 to 0.095 seconds.

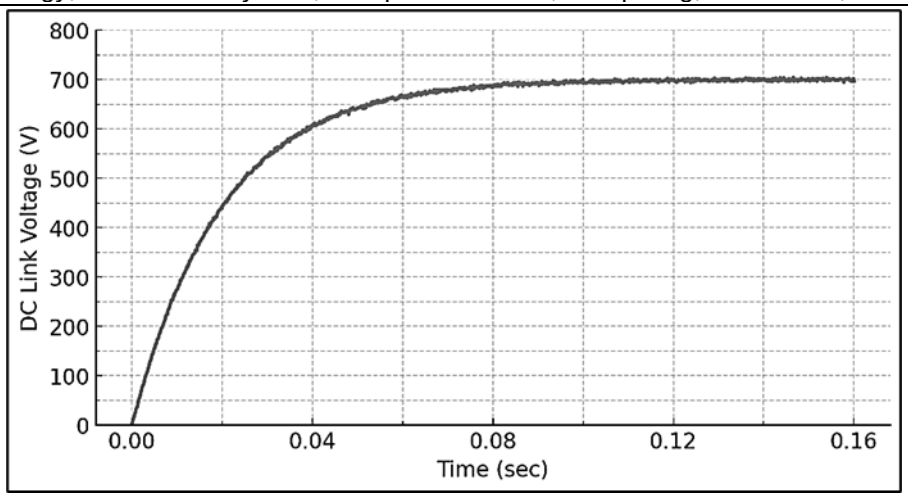

Figure 11. DC-link Voltage Waveform Controlled by FLC

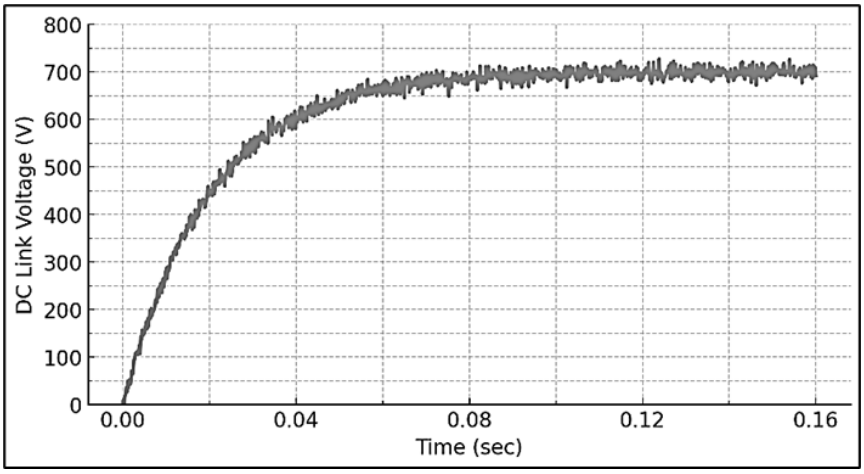

Figure 12. DC-link Voltage Waveform Controlled by PI

Figures 13 and 14 illustrate the over-frequency situation when the grid frequency rises to 51 Hz. Initially, the inverter operates in standalone mode, indicated by zero grid current. At 0.03 seconds, the inverter is connected to the grid. When the disturbance is detected between 0.06 and 0.09 seconds, the inverter disconnects from the grid and is shut down at 0.113 seconds. The isolation time, which is the duration from the occurrence of the disturbance to grid disconnection, is approximately 2.65 cycles. This complies with the IEEE Std. 929-2000 standard. As shown in Figure 14, from 0.113 seconds onward, the inverter voltage and the current supplied by the grid become zero, indicating that the inverter has been shut down according to the grid isolation algorithm for safety protection.

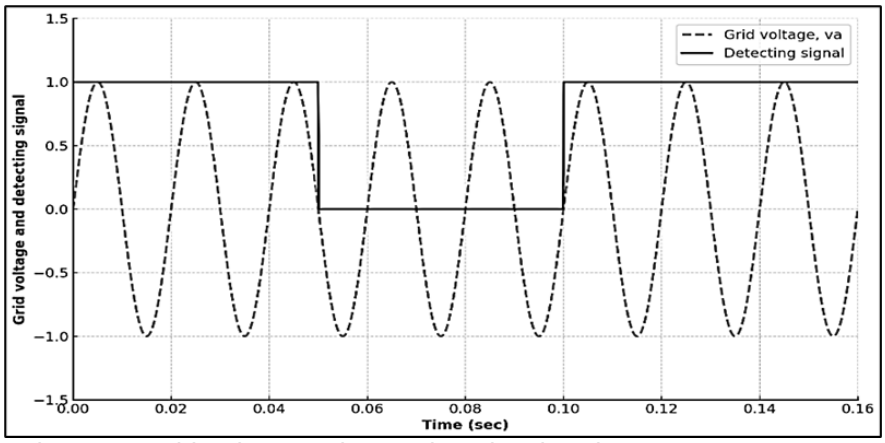

Figure 13. Grid Voltage and Detecting Signal During Frequency Increase

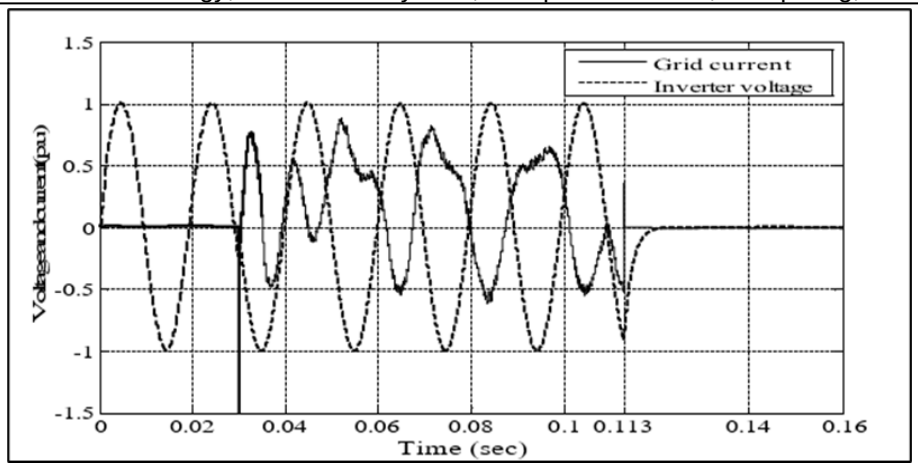

Figure 14. Grid Current and Inverter Voltage for Grid Frequency Increase

Figures 15 and 16 depict the under-frequency scenario when the grid frequency drops to 49 Hz. The inverter begins operation in standalone mode with zero grid current, then connects to the grid at 0.03 seconds. The inverter detects the disturbance at 0.065 seconds, and then disconnects from the grid and shuts down at 0.118 seconds. The disconnection and isolation process takes approximately 2.65 cycles, similar to the over-frequency case, and complies with the IEEE Std. 929-2000 standard. As with the over-frequency scenario, the under-frequency disturbance must be managed properly to ensure equipment protection and personnel safety. Figure 16 shows that after 0.118 seconds, the inverter voltage and the current supplied by the grid become zero because the inverter has been shut down according to the grid isolation algorithm.

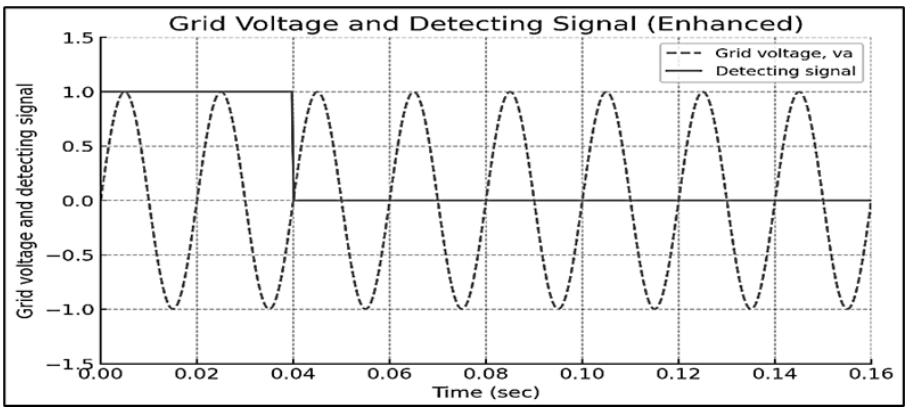

Figure 15. Grid Voltage and Detecting Signal During Frequency Decrease

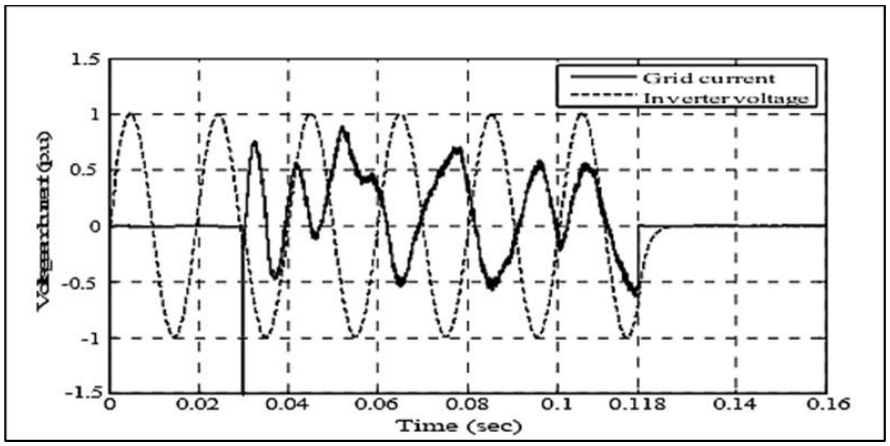

Figure 16. Grid Current and Inverter Voltage for Grid Frequency Decrease

Figures 17 and 18 show the inverter's response to a grid voltage increase to 264 V. Initially operating in standalone mode, the inverter connects to the grid at 0.03 seconds. When an over-voltage disturbance is detected at 0.0625 seconds, the inverter disconnects and shuts down, resulting in zero current flow and terminal voltage, as shown in Figure 18.

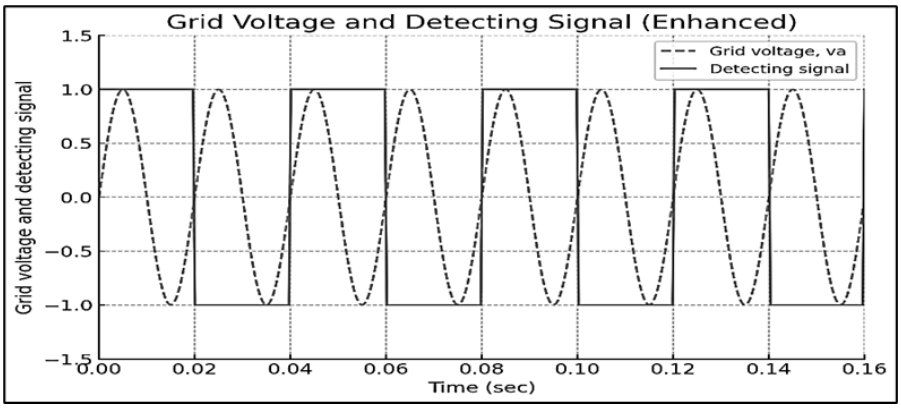

Figure 17. Detecting Signal for Grid Voltage Increase

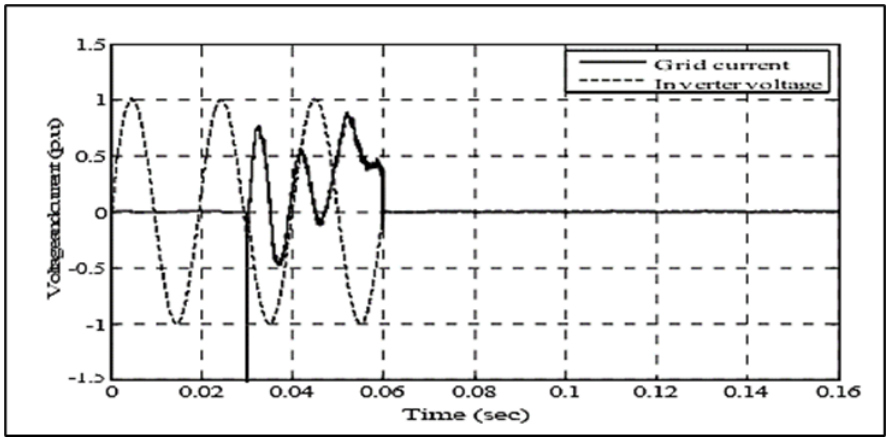

Figure 18. Grid Current and Inverter Voltage During Grid Voltage Increase

The behavior of the inverter when the grid voltage drops to 211 Vrms is shown in Figures 19 and 20. Initially, the inverter operates in standalone mode, then begins connecting to the grid at 0.03 seconds, indicated by the 'high' voltage level on the detection signal. A low-voltage disturbance occurs on the grid at 0.065 seconds. When the disturbance is detected, the control system changes the detection signal to 'low,' disconnecting and shutting down the inverter immediately. As a result, no current flows from the grid, and the voltage at the inverter terminals drops to zero, as seen in Figure 20.

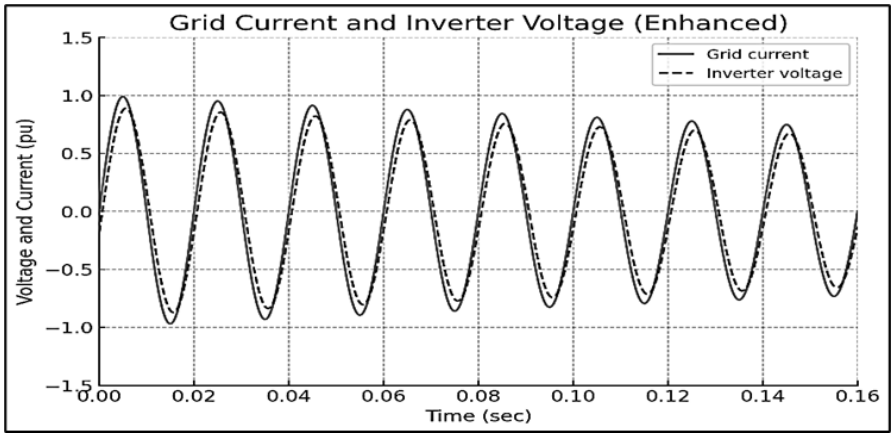

Figure 19. Inverter Voltage and Grid Current for Grid Voltage Decrease

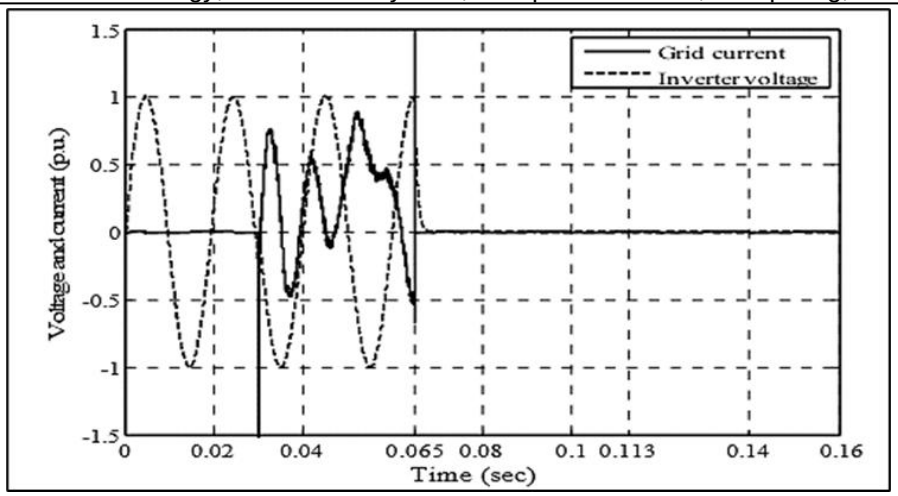

Figure 20. Grid Current and Inverter Voltage During Grid Voltage Decrease

The transient behavior of the grid current during the connection period with the inverter shows reductions and distortions when there are increases or decreases in frequency and voltage. This is due to the increased load demand causing the grid current and inverter voltage to be out of phase by 180º. Generally, the grid requires sinusoidal AC current with stable voltage and frequency. However, this test is conducted under varying frequency and voltage conditions to assess the controller's efficiency. When deviations from nominal conditions are detected, the control algorithm isolates the PV-based inverter system from the grid and immediately shuts down the inverter.

The application of the FLC control method on the inverter delivers a faster voltage response compared to the method proposed in previous research[27]. Table 2 presents the data on the FLC controller's response in comparison to the earlier method. Additionally, it also highlights the comparison of voltage and power stability within the microgrid system.

Table 2. Response Time for AC Bus Voltage

Controller type	Rise time/tr (s)	Settling time/ts (s)	Overshoot/Mp (%)
PID controller	0.042	0.85	17.38
FLC	0.015	0.50	0.50

Table 3. Fuzzy Logic Control on Inverter

Parameter	PID controller	FLC
DG unit power of PV	155 kW	158 kW
Battery power	150 kW	155 kW
AC bus voltage	374 V	380 V
Deviasi bus voltage	6 V	0 V
Maximum load current	1.2%	0%

Table 2 shows the response data of the FLC controller compared to the previous method. Additionally, Table 3 presents a comparison of voltage and power stability within the microgrid system.

4. Conclusion

This paper details the development and real-world testing of a fuzzy logic controller specifically designed for high-performance control of a grid-connected three-phase PV inverter. The control algorithm was implemented in real-time using the DSP controller board DS1104. The prototype system has been tested under various load conditions and grid voltage and frequency disturbance scenarios. The testing results demonstrate that the inverter control system utilizing the Fuzzy Logic Controller (FLC) is highly effective in producing stable and nearly sinusoidal voltage and current waveforms. Additionally, the inverter can transfer excess PV power to the utility grid and effectively detect grid disturbances, allowing it to disconnect from the grid to protect both the device and personnel. Real-time testing confirms that the FLC-controlled PV inverter system can deliver high-quality PV power to the grid, maintain a unity power factor, and manage grid voltage and frequency disturbances effectively. Therefore, the developed control system proves to be both highly effective and practical for the prototype implementation of a grid-connected PV system using the DS1104 controller board.

References

[1] C. Zhang, X. Li, X. Xing, B. Zhang, R. Zhang, and B. Duan, "Modeling and Mitigation of Resonance Current for Modified LCL-Type Parallel Inverters with Inverter-Side Current Control," *IEEE Trans Industr Inform*, vol. 18, no. 2, pp. 932–942, Feb. 2022. https://doi.org/10.1109/TII.2021.3076090

[2] L. Zhang *et al.*, "A Sensorless Implementation of the Parabolic Current Control for Single-Phase Stand-Alone Inverters," *IEEE Trans Power Electron*, vol. 31, no. 5, pp. 3913–3921, May 2016. https://doi.org/10.1109/TPEL.2015.2464292

[3] M. G. Judewicz, S. A. Gonzalez, J. R. Fischer, J. F. Martinez, and D. O. Carrica, "Inverter-side current control of grid-connected voltage source inverters with LCL filter based on generalized predictive control," *IEEE J Emerg Sel Top Power Electron*, vol. 6, no. 4, pp. 1732–1743, Dec. 2018. https://doi.org/10.1109/JESTPE.2018.2826365

[4] S. Kwak, S. E. Kim, and J. C. Park, "Predictive Current Control Methods with Reduced Current Errors and Ripples for Single-Phase Voltage Source Inverters," *IEEE Trans Industr Inform*, vol. 11, no. 5, pp. 1006–1016, Oct. 2015. https://doi.org/10.1109/TII.2015.2463757

[5] Y. Sun, Y. Liu, M. Su, H. Han, X. Li, and X. Li, "Topology and Control of a Split-Capacitor Four-Wire Current Source Inverter with Leakage Current Suppression Capability," *IEEE Trans Power Electron*, vol. 33, no. 12, pp. 10803–10814, Dec. 2018. https://doi.org/10.1109/TPEL.2017.2771537

[6] C. Tan, Q. Chen, K. Zhou, and L. Zhang, "A Simple High-Performance Current Control Strategy for V2G Three-Phase Four-Leg Inverter with LCL Filter," *IEEE Transactions on Transportation Electrification*, vol. 5, no. 3, pp. 695–701, 2019. https://doi.org/10.1109/TTE.2019.2936684

[7] L. Zhang, B. Gu, J. Dominic, B. Chen, C. Zheng, and J. S. Lai, "A dead-time compensation method for parabolic current control with improved current tracking and enhanced stability range," *IEEE Trans Power Electron*, vol. 30, no. 7, pp. 3892–3902, Jul. 2015. https://doi.org/10.1109/TPEL.2014.2339302

[8] R. Viswadev, A. Mudlapur, V. V. Ramana, B. Venkatesaperumal, and S. Mishra, "A Novel AC Current Sensorless Hysteresis Control for Grid-Tie Inverters," *IEEE Transactions on Circuits and Systems II: Express Briefs*, vol. 67, no. 11, pp. 2577–2581, Nov. 2020. https://doi.org/10.1109/TCSII.2019.2960289

[9] A. Abdelhakim, P. Mattavelli, D. Yang, and F. Blaabjerg, "Coupled-Inductor-Based DC Current Measurement Technique for Transformerless Grid-Tied Inverters," *IEEE Trans Power Electron*, vol. 33, no. 1, pp. 18–23, Jan. 2018. https://doi.org/10.1109/TPEL.2017.2712197

[10] G. Qiu, J. Liao, B. Wu, and Z. Shi, "Suppressing DC Current Injection in Transformerless Grid-Connected Inverter Using a Customized Current Sensor," *IEEE Trans Power Electron*, vol. 36, no. 10, pp. 11003–11008, Oct. 2021. https://doi.org/10.1109/TPEL.2021.3071195

[11] B. Yu, W. Song, Y. Guo, J. Li, and M. S. R. Saeed, "Virtual Voltage Vector-Based Model Predictive Current Control for Five-Phase VSIs with Common-Mode Voltage Reduction," *IEEE Transactions on Transportation Electrification*, vol. 7, no. 2, pp. 706–717, Jun. 2021. https://doi.org/10.1109/TTE.2020.3030793

[12] C. A. Agustin, J. Te Yu, C. K. Lin, J. Jai, and Y. S. Lai, "Triple-Voltage-Vector Model-Free Predictive Current Control for Four-Switch Three-Phase Inverter-Fed SPMSM Based on Discrete-Space-Vector Modulation," *IEEE Access*, vol. 9, pp. 60352–60363, 2021. https://doi.org/10.1109/ACCESS.2021.3074067

[13] Q. Huang and A. Q. Huang, "Variable frequency average current mode control for zvs symmetrical dual-buck h-bridge all-gan inverter," *IEEE J Emerg Sel Top Power Electron*, vol. 8, no. 4, pp. 4416–4427, Dec. 2020. https://doi.org/10.1109/JESTPE.2019.2940270

[14] Z. Liang, X. Lin, Y. Kang, B. Gao, and H. Lei, "Short Circuit Current Characteristics Analysis and Improved Current Limiting Strategy for Three-phase Three-leg Inverter under Asymmetric Short Circuit Fault," *IEEE Trans Power Electron*, vol. 33, no. 8, pp. 7214–7228, Aug. 2018. https://doi.org/10.1109/TPEL.2017.2759161

[15] Z. Xin, P. Mattavelli, W. Yao, Y. Yang, F. Blaabjerg, and P. C. Loh, "Mitigation of Grid-Current Distortion for LCL-Filtered Voltage-Source Inverter with Inverter-Current Feedback Control," *IEEE Trans Power Electron*, vol. 33, no. 7, pp. 6248–6261, Jul. 2018. https://doi.org/10.1109/TPEL.2017.2740946

[16] H. C. Vu and H. H. Lee, "Model-Predictive Current Control Scheme for Seven-Phase Voltage-Source Inverter with Reduced Common-Mode Voltage and Current Harmonics," *IEEE J Emerg Sel Top Power Electron*, vol. 9, no. 3, pp. 3610–3621, Jun. 2021. https://doi.org/10.1109/JESTPE.2020.3009392

[17] A. T. Nguyen, S. W. Ryu, A. U. Rehman, H. H. Choi, and J. W. Jung, "Improved Continuous Control Set Model Predictive Control for Three-Phase CVCF Inverters: Fuzzy Logic Approach," *IEEE Access*, vol. 9, pp. 75158–75168, 2021. https://doi.org/10.1109/ACCESS.2021.3081718

[18] W. Song, C. Xue, X. Wu, and B. Yu, "Modulated Finite-Control-Set Model Predictive Current Control for Five-Phase Voltage-Source Inverter," *IEEE Transactions on Transportation Electrification*, vol. 7, no. 2, pp. 718–729, Jun. 2021. https://doi.org/10.1109/TTE.2020.3019208

[19] M. Hofmann, M. Schaefer, D. Montesinos-Miracle, and A. Ackva, "Improved Direct Current Control for Grid-Connected Multilevel Inverters," *IEEE Transactions on Industrial Electronics*, vol. 68, no. 9, pp. 8289–8297, Sep. 2021. https://doi.org/10.1109/TIE.2020.3018055

[20] I. Rullah, R. K. Harahap, E. P. Wibowo, A. I. Sukowati, D. Nur'ainingsih, and W. Widyastuti, "Design and Simulation of Low Power and Voltage Micro Photovoltaic Cell for Mobile Devices," *Kinetik: Game Technology, Information System, Computer Network, Computing, Electronics, and Control*, Feb. 2022. https://doi.org/10.22219/kinetik.v7i1.1355

[21] M. A. Hannan, Z. A. Ghani, A. Mohamed, and M. N. Uddin, "Real-Time Testing of a Fuzzy-Logic-Controller-Based Grid-Connected Photovoltaic Inverter System," *IEEE Trans Ind Appl*, vol. 51, no. 6, pp. 4775–4784, Nov. 2015. https://doi.org/10.1109/TIA.2015.2455025

[22] A. Kusmantoro, "Multi-Inverter Coordinated Control on AC Microgrid for Increased Load Power," in *2023 6th International Conference on Vocational Education and Electrical Engineering: Integrating Scalable Digital Connectivity, Intelligence Systems, and Green Technology for Education and Sustainable Community Development, ICVEE 2023 - Proceeding*, Institute of Electrical and Electronics Engineers Inc., 2023, pp. 90–95. https://doi.org/10.1109/ICVEE59738.2023.10348326

[23] H. Jafarian, R. Cox, J. H. Enslin, S. Bhowmik, and B. Parkhideh, "Decentralized Active and Reactive Power Control for an AC-Stacked PV Inverter with Single Member Phase Compensation," in *IEEE Transactions on Industry Applications*, Institute of Electrical and Electronics Engineers Inc., Jan. 2018, pp. 345–355. https://doi.org/10.1109/TIA.2017.2761831

[24] Y. Yang, K. Zhou, and F. Blaabjerg, "Current Harmonics from Single-Phase Grid-Connected Inverters-Examination and Suppression," *IEEE J Emerg Sel Top Power Electron*, vol. 4, no. 1, pp. 221–233, Mar. 2016. https://doi.org/10.1109/JESTPE.2015.2504845

[25] P. Alemi, C. J. Bae, and D. C. Lee, "Resonance Suppression Based on PR Control for Single-Phase Grid-Connected Inverters With LLCL Filters," *IEEE J Emerg Sel Top Power Electron*, vol. 4, no. 2, pp. 459–467, Jun. 2016. https://doi.org/10.1109/JESTPE.2015.2464699

[26] J. Xu, S. Xie, B. Zhang, and Q. Qian, "Robust Grid Current Control with Impedance-Phase Shaping for LCL-Filtered Inverters in Weak and Distorted Grid," *IEEE Trans Power Electron*, vol. 33, no. 12, pp. 10240–10250, Dec. 2018. https://doi.org/10.1109/TPEL.2018.2808604

[27] A. Kusmantoro and I. Farikhah, "Power management on DC microgrid with new DC coupling based on fuzzy logic," *Indonesian Journal of Electrical Engineering and Computer Science*, vol. 32, no. 2, pp. 620–631, Nov. 2023. https://doi.org/10.11591/ijeecs.v32.i2.pp620-631